# Patterns in bistable resonant-tunneling structures

B. A. Glavin and V. A. Kochelap

*Institute of Semiconductor Physics, Ukrainian Academy of Sciences, Pr. Nauki 45, Kiev 252028, Ukraine*

V. V. Mitin

*Electrical and Computer Engineering Department, Wayne State University, Detroit, Michigan 48202*

(Received 20 November 1996)

We report a theoretical investigation of the phenomenon of the formation of patterns transverse to the tunneling current in resonant-tunneling double-barrier heterostructures. Such patterns arise in heterostructures with an intrinsic bistability of the current-voltage characteristic. The patterns are characterized by a nonuniform distribution of resonant electrons in the quantum-well layer and, consequently, a nonuniform tunneling current density through the heterostructure. Patterns exist for coherent and for sequential mechanisms of the resonant tunneling. Possible types of stationary patterns depend on the applied voltage, and can be controlled by conditions on the edges of the heterostructure. In fact, the patterns are two or three dimensional in character, since the nonuniform electron distributions induce a complex configuration of the electrostatic potential in barrier regions. In addition to stationary patterns, moving patterns are considered. They describe the switching of the heterostructure from one uniform state to another. [S0163-1829(97)05544-6]

## I. INTRODUCTION

Resonant tunneling through a double-barrier heterostructure was observed two decades ago,[1] but this phenomenon still attracts considerable interest because of its fundamental character and increasing number of prospective applications (microwave oscillations,[2] circuit applications,[3,4] cascade lasers,[5,6] etc). A resonant quasibound state is formed in a quantum well between two barriers. These barriers separate the well from electrodes (heavy doped emitter and collector regions). The energy of the quasibound state, measured with respect to the bottom of the quantum well, $\varepsilon_0$, is usually chosen to be above the Fermi level $E_F$ of electrodes when no voltage is applied. The applied bias shifts the energy of quasibound state below $E_F$, and the electric current passes mostly through the quasibound state. The current increases with the bias until the energy of the quasibound state lowers below the bottom $E_0$ of the emitter band. At this region the current falls to a low value, and negative differential resistance occurs. Different particular mechanisms can be responsible for the resonant tunneling (coherent,[7] sequential,[8] phonon-assisted mechanisms,[9,10] etc.). However, when the quasibound state is in resonance with the emitter electron states, there is a finite density of electrons, i.e., a built-up charge, in the quantum well. This built-up charge determines the voltage distribution across the heterostructure, and considerably affects the current-voltage characteristic. The other important effect induced by the built-up charge is the intrinsic bistability of the system under consideration. For some range of biases at a fixed bias, two stable states exist. One state is characterized by the large built-up charge, resonant-tunneling conditions, and a large current; the other one corresponds to resonance breaking, a lowering of the quasibound state below the bottom of the emitter band, and a low built-up charge and current.

The possibility of electrical instability due to an accumulation of the charge in the well was pointed out by Ricco and

Azbel.[11] Subsequently, the intrinsic bistability was observed by a number of experimental groups[12–14] for various double-barrier structures. Calculations and modeling of the bistability were done by various authors.[15–17]

In these papers, the tunneling was considered one dimensional, and the transport through the double-barrier heterostructure was supposed to be dependent on only one coordinate, perpendicular to the barriers. Actually, most double-barrier resonant tunneling structures are layered ones, and the tunneling electron can move not only across the layers (vertical transport), but also along these layers (horizontal, or lateral, transport). Because the applied voltage is uniformly distributed over the highly conductive emitter and collector regions, a one-dimensional picture of the electron transport through barriers and quantum-well layers is sufficient for regimes with a single state (note, however, that transverse patterns in this case are possible in the structures with special conditions on their boundaries[18]). However, for the case of bistability, different states of the nonequilibrium system can coexist. This leads to nonuniform (in the plane of the layers) distributions of the tunneling current, and built-up charge and potential energy. That is, under a bistable tunneling regime one can expect spontaneous formation of transverse patterns.

There is a well-known analogy between light waves in the Fabry-Perot interferometer and the electron waves in double-barrier structures. The analogy qualitatively illustrates the resonant behavior of electron transmission through the structures. The analogy can be extended to the bistability regimes. A medium with optical nonlinearity, embedded inside a resonator, gives rise to optical bistability or multistability.[19] Under these conditions, different stationary and moving transversal patterns are realized.[19,20] In the case of tunneling, nonlinearity in the wave equation appears due to electrostatic interaction. Similarly to a nonlinear interferometer, one can imagine various transverse patterns for tunneling in double-barrier structures. In contrast to the case of a nonlinear inter-

ferometer, the patterns of resonant tunneling can appear for both types of tunneling, coherent and incoherent. One of the goals of this paper is to demonstrate the possibility of these patterns.

There are a variety of self-consistent patterns known in solid-state physics: stationary and moving Gunn domains, and current filaments at $N$- and $S$-shaped current-voltage characteristics, respectively;[21] transverse domains in semiconductors with equivalent valleys;[22,23] stationary and wave patterns under resonatorless optical bistability;[24,25] etc. These and other known examples are related to nonlinear classical electron transport, while, for the case analyzed in this paper, at least in the vertical direction, the transport has a quantum character.

Since horizontal electron transfer is the main process determining the transverse patterns, let us consider it qualitatively. This transfer can be depicted as follows. The electron is injected from the emitter to the well in general with a finite horizontal component of the momentum $p$ or velocity $v = p/m^*$ ($m^*$ is the effective mass). The velocity depends on the position of the quasibound-state energy with respect to the Fermi energy $E_F$ in the emitter: when the energy quasibound level moves from $E_F$ through the bottom of the emitter band $E_0$, the velocity changes from zero to the Fermi velocity $v_F = \sqrt{2E_F/m^*}$. For estimates, one can say that $v$ and $v_F$ have the same order of magnitude. We can introduce a characteristic time for horizontal transfer: a time of tunneling escape from the well $\tau_{es}$. The characteristic distance of the horizontal transfer is $L_{ch} = v\tau_{es}$. One can expect that the scale of the patterns in question is of the order of $L_{ch}$.

For sharp resonant level from the uncertainty relation for the quasibound state we can write $\varepsilon_0\tau_{es} \gg \hbar$. Combining this inequality with the fact, that $E_F$, $\varepsilon_0$, and the kinetic energy of the horizontal motion $m^*v^2/2$ are of the same order of magnitude, for the in-plane wave vector $k$ we find

$$kL_{ch} = \frac{p}{\hbar} L_{ch} = \frac{m^*v^2}{\hbar} \tau_{es} \sim \varepsilon_0\tau_{es} \gg 1.$$

The latter estimate shows that horizontal transfer can be considered as classical. Based on this conclusion, we develop a theory of the patterns, assuming that the vertical transport is quantum and the horizontal transfer is classical. From the same uncertainty condition we can deduce that the characteristic scale $L_{ch}$ greatly exceeds the well width. We assume $L_{ch}$ is much larger than the thickness of the whole structure:

$$L_{ch} \gg d. \tag{1}$$

The paper is organized as follows. In Sec. II the model and basic equations necessary for an investigation of the patterns are given. In Sec. III we show the existence of bistability for uniform tunneling within the proposed model. An analysis of the patterns for the limiting case where a local approach to electron transport is applicable, is done in Sec. IV. A more general consideration based on the kinetic equation is presented in Sec. V. Section VI summarizes the main results of the paper. The derivation of some necessary equations, and methods of their simplification, are presented in Appendixes A–D.
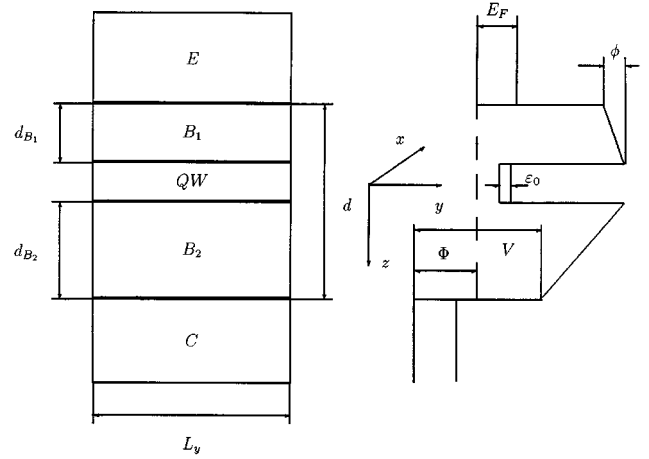


FIG. 1. The scheme and energy-band diagram of the resonant-tunneling structure.

## II. MODEL AND BASIC EQUATIONS

Since the problem of the transverse patterns requires at least a two-dimensional spatial analysis, we use a simple model, showing the main features of the bistability and the patterns. We deal with the model of a resonant-tunneling heterostructure, schematically shown in Fig. 1. The structure is treated as a system of three parts, weakly coupled by tunneling: emitter ($E$), quantum well (QW), and collector ($C$). The electrodes $E$ and $C$ are usually heavy doped semiconductors, and are supposed to be ideal conductors with zero screening length. The energy height of the barriers $B_1$, and $B_2$ is $V$, and their thicknesses are $d_{B_1}$ and $d_{B_2}$ respectively.

Charge accumulation in the well causes a change of the potential profile in the whole structure. It alters the position of the quasibound state with respect to the bottom of the energy band of the emitter and, in general, with respect to the bottom of the quantum well. We disregard the latter effect, and consider that the built-up charge shifts the well bottom and the quasibound level equally. Such a case corresponds to the very thin quantum well, where the built-up charge can be accounted for as an infinitely thin sheet. The thinner the well is with respect to $d_{B_1}$ and $d_{B_2}$, the better our model describes the real structure.

Introducing the area concentration $n$ of electrons in the well, for the assumption discussed above we can write the Poisson equation in the form

$$\Delta\varphi = -\frac{4\pi e^2}{\kappa} \delta(z)n(\mathbf{r}) \tag{2}$$

where $\varphi(\mathbf{r},z)$ is the electrostatic potential energy for electrons, $\mathbf{r} = \{x,y\}$, $\kappa$ is the dielectric constant, and $e$ is the elementary electric charge. The coordinate system is shown in Fig. 1. The boundary conditions at the electrodes are

$$\varphi(\mathbf{r},z=-d_{B_1}) = 0, \quad \varphi(\mathbf{r},z=d_{B_2}) = -\Phi, \tag{3}$$

where $\Phi$ is the external voltage bias in energy units.

Under the conditions of weak coupling between emitter, quantum well, and collector, for the electron distribution

function in the well $f(\mathbf{r},\mathbf{p},t)$ one can derive the Boltzmann-like kinetic equation [see Appendix A, Eq. (A5)]

$$\frac{\partial f}{\partial t} + \frac{\mathbf{p}}{m^*} \frac{\partial f}{\partial \mathbf{r}} - \frac{\partial \phi}{\partial \mathbf{r}} \frac{\partial f}{\partial \mathbf{p}} = G[\phi(\mathbf{r},t),\mathbf{p}] - \frac{f}{\tau_{es}} + I\{f\}, \quad (4)$$

where $\mathbf{p}$ is two-dimensional momentum, $\phi(\mathbf{r}) \equiv \varphi(\mathbf{r}, z=0)$ is the electrostatic potential energy in the well, $G[\phi(\mathbf{r},t),\mathbf{p}]$ is the local rate of tunneling from the emitter to the well, $\tau_{es}$ is the tunneling escape time, and $I\{f\}$ is the collision integral for the electrons inside the well. As we stated in Sec. I, lateral transport of resonant electrons is classical, which is reflected in the semiclassical character of Eq. (4). One can see that Eq. (4) is a conventional Boltzmann equation with two additional terms on the right-hand side: $G$ and $-f/\tau_{es}$. The first of these describes tunnel injection of electrons from the emitter to the quantum well, and the second one describes the tunnel escape of electrons from the quantum well to the electrodes. The classical character of the lateral transport is reflected once more in the local character of tunneling injection and escape terms: $G$ and $\tau_{es}$ are functions of $\phi$ at fixed $\mathbf{r}$. They are expressed through the tunneling probabilities and the Fermi distribution of electrons in the emitter (see Appendix A). If these functions are known, Eqs. (2) and (4), along with the definition of concentration

$$n(\mathbf{r},t) = \sum_{\mathbf{p}} f(\mathbf{r},\mathbf{p},t), \quad (5)$$

compose the system of coupled nonlinear equations. Besides the boundary conditions at the electrodes [Eq. (3)], additional boundary conditions have to be imposed in the $x,y$ plane.

We can considerably simplify the system using inequality (1). Then the differential equation (2) with boundary conditions of Eq. (3) can be presented in the integral form of Eq. (B1) as an equation for $\phi$:

$$\phi = -\frac{d_{B_1}}{d} \Phi + \int d\mathbf{r}' K(\mathbf{r}-\mathbf{r}') n(\mathbf{r}'). \quad (6)$$

The kernel function $K(\mathbf{r})$ is calculated in Appendix B. From Eqs. (B4) and (B5) one can see that $K(\mathbf{r})$ has a maximum at $\mathbf{r}=0$, and decays almost exponentially with characteristical length of the order of $d$. Since the spatial scale of the function $n(\mathbf{r})$ is $L_{ch}$, using Eq. (1) we can approximate

$$\int d\mathbf{r}' K(\mathbf{r}-\mathbf{r}') n(\mathbf{r}') \approx n(\mathbf{r}) \int d\mathbf{r}' K(\mathbf{r}-\mathbf{r}').$$

As a result, we obtain the solution of the electrostatic problem,

$$\phi(\mathbf{r}) = -\frac{d_{B_1}}{d} \Phi + \frac{4\pi e^2}{\kappa} \frac{d_{B_1} d_{B_2}}{d} n(\mathbf{r}). \quad (7)$$

Let us discuss the boundary conditions in the $x,y$ plane. For a heterostructure with infinite horizontal dimensions, we require finite magnitudes of solutions at $x,y \to \pm\infty$. For restricted horizontal dimensions, different kinds of effects determine the boundary conditions. The simplest is a straightforward scattering of electrons at the edges of the quantum

well. Such an edge scattering can be considered analogously to the case of thin metal layers, etc.[26,27] For two-dimensional electrons limiting cases of diffusive and specular boundary scattering were studied in Refs. 26 and 27. Also, parameters of the system at the edges (thicknesses of the barriers and the well, etc.) can be different from those ones in the bulk. If these changes are localized in a region that is small with respect to $L_{ch}$, they also can be included in the boundary conditions.

## III. BISTABILITY UNDER UNIFORM TUNNELING

Let us show that the model formulated above allows bistable vertical transport regimes with uniform tunneling in the $x,y$ plane. In such a case the $\mathbf{r}$ and $t$ dependences are absent, and, from the kinetic equation (4), one can find the areal electron concentration

$$n(\phi) = \tau_{es}(\phi) g(\phi). \quad (8)$$

Since the left-hand side of Eq. (8) is a function of $\phi$, we obtain two algebraic equations (7) and (8) for two variables $n$ and $\phi$. It is convenient to rewrite this system as

$$L(\phi) \equiv n(\phi) = \frac{\kappa d}{4\pi e^2 d_{B_1} d_{B_2}} \left( \phi + \frac{d_{B_1}}{d} \Phi \right) \equiv R(\phi). \quad (9)$$

For the particular heterostructure the latter equation has one controlling parameter: the external bias $\Phi$. The right-hand side is a linear function of $\phi$ and $\Phi$. The left one is more complicated function, having, generally, a superlinear dependence in the bias range, where the quasibound level crosses the bottom of the emitter band. This dependence can generate more than one solution of Eq. (9).

We calculated the functions $\tau_{es}(\phi)$ and $g(\phi)$ for a heterostructure with parameters (structure I) $V=1$ eV, $m^* = 0.067 m_0$, $d=5.8$ nm, $d_{B_1}=2$ nm, $\varepsilon_0 = 0.1$ eV, $\kappa = 11.5$, and a scattering broadening of the quasi-bound-state of 0.054 meV. In Fig. 2 the left- and right-hand sides are shown for $E_F = 56$ meV and zero temperature. Cases (a)–(c) correspond to different biases $\Phi$. The dependences $n(\phi)$ can be understood as follows. Because the energy $\varepsilon_0$ exceeds the Fermi level $E_F$ at high $\phi$, the injection of the carriers into the well is small, and the built-up concentration is low. If $\phi$ is negative and decreases, the quasibound state is shifted down and the concentration increases. At high negative $\phi$ the resonant state descends below the emitter band bottom, the concentration sharply drops down in accordance with qualitative consideration. This results in a superlinear dependence $n(\phi)$ [see Figs. 2(a)–2(c)]. This dependence changes only weakly with the total bias $\Phi$. This means that the main control parameter dependence comes from the right-hand side of Eq. (9). For voltage biases $\Phi < \Phi_l$, only one solution with a high electron concentration exists. At $\Phi \approx \Phi_l \approx 0.285$ eV, the second solution with a low concentration appears [Fig. 2(a)]. In the range $\Phi_l < \Phi < \Phi_h \approx 0.318$ eV three solutions exist, and are well separated [Fig. 2(b)]. Two of them are stable; they correspond to the bistable regime of tunneling. At $\Phi \approx \Phi_h$ two high-density solutions coalescence [Fig. 2(c)], and disappear at $\Phi > \Phi_h$. The electron current through the heterostructure is shown in Fig. 3. In the bistability range the
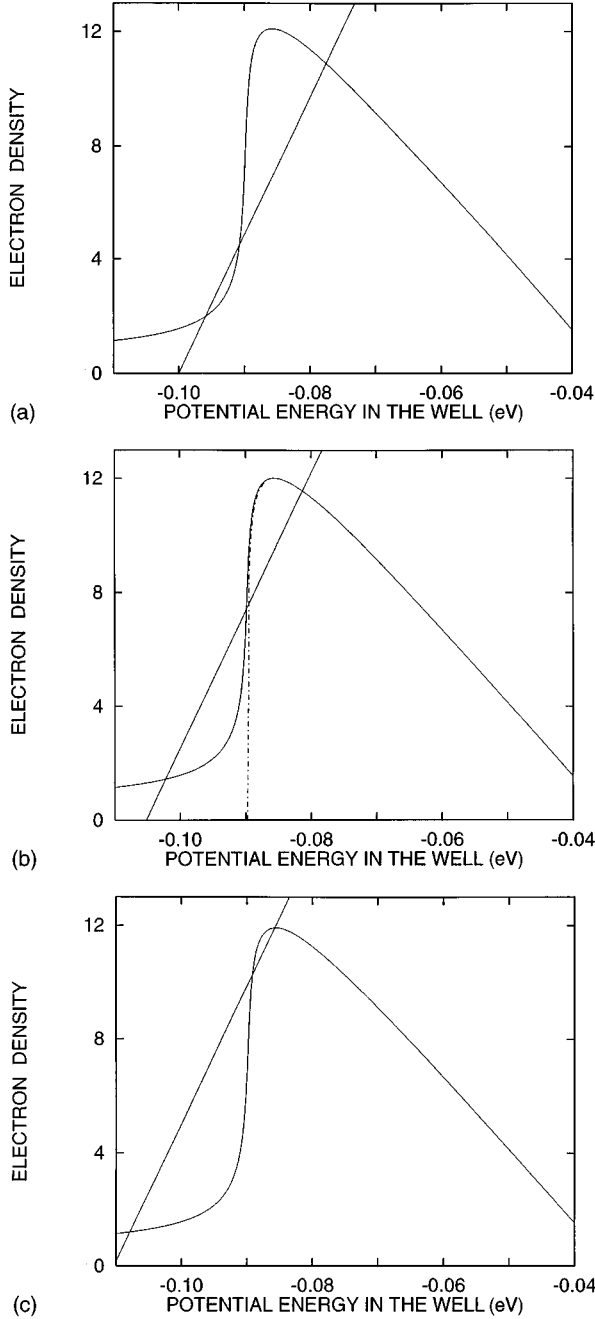
FIG. 2. Self-consistent solutions of the bistability problem under uniform tunneling for structure I: the right and left sides of Eq. (9) are shown separately. (a) $\Phi = 0.29$ eV. (b) $\Phi = 0.305$ eV. The dotted line shows the dependence $n_0(\phi)$, in the limit of zero broadening of the resonant level. (c) $\Phi = 0.32$ eV.

current-voltage characteristic has a $Z$-type shape; the high and low currents can be realized at the same voltage bias.

If one assumes the resonant level to be infinitely sharp [the corresponding $n(\phi)$ dependence is shown in Fig. 2(b)], it is possible to analyze the dependence of the bistability range on the parameters of the heterostructure. For this purpose we introduce two dimensionless parameters

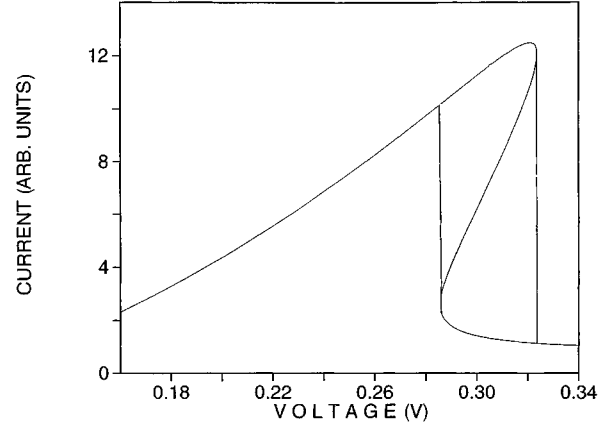$$k = \frac{\tau_{cw}\tau_{sc}}{\tau_{ew}(\tau_{cw} + \tau_{sc})}, \tag{10}$$



FIG. 3. $Z$-shaped current-voltage characteristic of structure I.

$$\sigma = \frac{\kappa d\hbar^2}{4e^2 d_{B_1} d_{B_2} m^*}, \tag{11}$$

where the tunneling times $\tau_{ew}$ and $\tau_{cw}$ are calculated at $\varepsilon = E_F$, $\tau_{sc}$ is the scattering time (see Appendix C, where we introduce $\tau_{sc}$). In this case the dimensionless range of bistability $q \equiv (\Phi_h - \Phi_l)/E_F$ can be evaluated as a function of $k$ and $\sigma$. Note that $\sigma$ can be expressed through the effective Bohr radius $a_B$ in the material of the system: $\sigma = a_B^2/4d_{B_1}d_{B_2}$. In Fig. 4 the dependence $q(k)$ is shown at $\sigma = 1.7$. According to Fig. 4, bistability exists at any $k$. But the bistability is more developed for asymmetric heterostructures, for which $\tau_{ew} < \tau_{sc}\tau_{cw}/(\tau_{cw} + \tau_{sc})$. This fact explains the dependence of the bistability on the temperature, which is usually observed in experiments: at higher temperatures $\tau_{sc}$ decreases, and this washes out the asymmetry of tunneling in the system. Note that a large bistability range is possible even for completely incoherent resonant tunneling, when $\tau_{sc} \ll \tau_{cw}$, but $\tau_{ew} < \tau_{sc}$

## IV. PATTERNS IN THE LOCAL APPROACH FOR THE HORIZONTAL TRANSFER

In Appendix C it is shown that sufficiently smooth transverse distributions of the electrons can be described by the diffusionlike differential equation (C13), combined with the
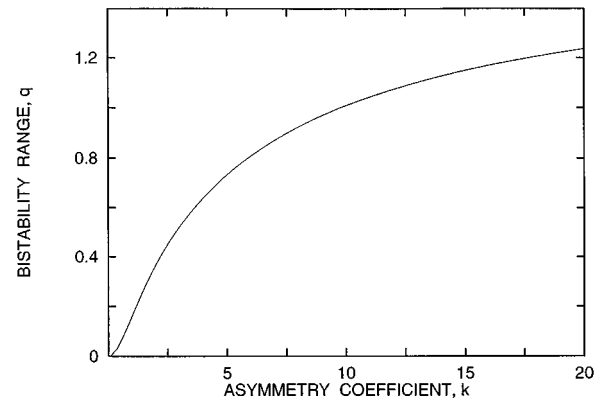


FIG. 4. Dependence of the bistability range $q = (\Phi_h - \Phi_l)/E_F$ on the coefficient of asymmetry of the barriers $k$ for $\sigma = 1.7$.

solution
of electrostatical problem of Eq. (7). To avoid cumbersome formulas, we introduce functions

$$\mathcal{D}(\phi) = \frac{4\pi e^2}{\kappa} \frac{d_{B_1} d_{B_2}}{d} D(\phi), \tag{12}$$

$$\mathcal{R}(\phi) = \frac{4\pi e^2}{\kappa} \frac{d_{B_1} d_{B_2}}{d} g(\phi) - \frac{1}{\tau_{es}(\phi)} \left( \phi + \frac{d_{B_1}}{d} \Phi \right). \tag{13}$$

Then, for $\phi$ we obtain the equation with the nonlinear diffusivity and the source-drain term:

$$\frac{\partial \phi}{\partial t} = \frac{\partial}{\partial \mathbf{r}} \left( \mathcal{D}(\phi) \frac{\partial \phi}{\partial \mathbf{r}} \right) = \mathcal{R}(\phi). \tag{14}$$

In Eq. (14) we neglect by the difference between $\partial n_0(\phi)/\partial t$ and $\partial n/\partial t$ because the difference has a higher order of magnitude for smooth patterns.

At the edges of the quantum well, $\mathbf{r} = \mathbf{r}_e$, we should impose boundary conditions. In the local approach these conditions can be written in the form of conditions on the horizontal flux at the edges:

$$j_n = S(n_e - n), \quad \mathbf{r} = \mathbf{r}_e. \tag{15}$$

Here $j_n$ is normal component of current (C10). These boundary conditions take into account the fact that, near the edges for distances much less than $L_{ch}$, the injection and escape rates can differ from those in the bulk of the well layer. In general, the parameters $S$ and $n_e$ depend on $\mathbf{r}$. In the terms of the functions introduced in Eqs. (12) and (13), the boundary conditions for $\phi$ are

$$\mathcal{D}(\phi) \left( \frac{\partial \phi}{\partial \mathbf{r}} \right)_n = S(\phi_e - \phi), \quad \phi_e = \frac{4\pi e^2}{\kappa} \frac{d_{B_1} d_{B_2}}{d} n_e, \quad \mathbf{r} = \mathbf{r}_e. \tag{16}$$

For transverse patterns with a characteristical length $L_{st}$, Eq. (14) and boundary conditions of Eq. (16) are valid for

$$L_{st} \gg v_F \tau_{es}. \tag{17}$$

Below we analyze this requirement.

We restrict ourselves to a consideration of one-dimensional patterns depending on $y$ only. In this case for the stationary patterns we find

$$-\frac{\partial}{\partial y} \left( \mathcal{D}(\phi) \frac{\partial \phi}{\partial y} \right) = \mathcal{R}(\phi). \tag{18}$$

The first and second integrals of Eq. (18) are

$$\frac{d\phi}{dy} = \pm \frac{1}{\mathcal{D}(\phi)} \sqrt{-2 \int_{\phi_0}^{\phi} \mathcal{D}(\phi') \mathcal{R}(\phi')}, \tag{19}$$

$$\int_{\phi_0}^{\phi} \frac{\mathcal{D}(\phi') d\phi'}{\sqrt{-2 \int_{\phi_0}^{\phi'} d\phi'' \mathcal{D}(\phi'') \mathcal{R}(\phi'')}} = \pm(y - y_0), \tag{20}$$

respectively. Here $\phi_0$ and $y_0$ are two integration constants.

The simplest way to classify possible types of implicit solutions of Eqs. (19) and (20) is to employ phase portrait
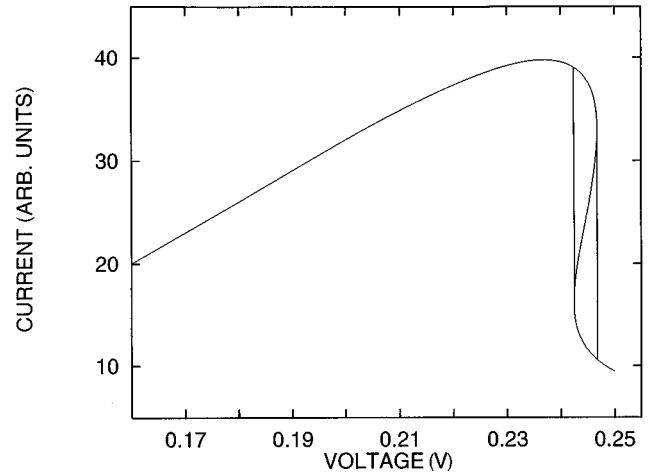


FIG. 5. Z-shaped current-voltage characteristic of structure II.

analysis. It is easy to see that the uniform solutions of Eq. (9), studied in Sec. III, correspond to zeros of $\mathcal{R}(\phi)$ and, consequently, to the singular points of the phase plane ($\phi - d\phi/dy$). In the bistable range of the bias, $[\Phi_l, \Phi_h]$, there are three or two (for $\Phi = \Phi_l, \Phi_h$) singular points.

As we shall see below, the local approach is valid for all $\Phi$ within the bistability range only in the case of a weak bistability. Here we deal with a structure (structure II) with values of barrier thicknesses and scattering broadening different from those used in Sec. III: $d_{B_1} = 2$ nm, $d_{B_2} = 3$ nm, and the scattering broadening 0.35 meV. The current-voltage characteristic of this structure is shown in Fig. 5.

In Fig. 6 the phase portraits of Eq. (18) are shown for structure II for external bias $\Phi$ within the bistable range. In fact, the phase portraits represent possible solutions of Eq. (18) on the $\phi - (d\phi/dy)$ plane. For all cases the two singular points (the left $\phi_l$ and the right $\phi_r$) are saddles, while the middle one $\phi_m$ is the center; $s$ and $s'$ label the separatrixes. Cases (a)–(c) differ in the behavior of the separatrixes. For case (a) one of the separatrixes ($s$) originates from the right saddle, and finishes in the same saddle forming the closed trajectory. Case (b) is very special one, where two separatrixes, $s$ and $s'$ connect the saddles. Case (c) is similar to case (a), but the closed separatrix originates from the left saddle. For all these cases the separatrixes isolate the region of the plane with closed trajectories. These closed trajectories and separatrixes correspond to solutions which are finite in space even for $|y| \rightarrow \infty$. They describe patterns in heterostructures with infinitely large transverse dimensions. The closed trajectories (other then separatrixes) give periodical patterns. The separatrixes correspond to the aperiodical patterns: soliton type (a), antisoliton type (c), and kinklike (b). Spatial dependences of the electron density, corresponding to the aperiodical patterns, are shown in Fig. 7. The kinklike pattern occurs at unique bias $\Phi_c$, which can be obtained from the first integral (19):

$$\int_{\phi_l}^{\phi_r} d\phi \mathcal{D}(\phi, \Phi_c) \mathcal{R}(\phi, \Phi_c) = 0. \tag{21}$$

Note that Eq. (21) is the analog of the "rule of equal areas," which is valid for many nonequilibrium patterns of different origin.[21–25]
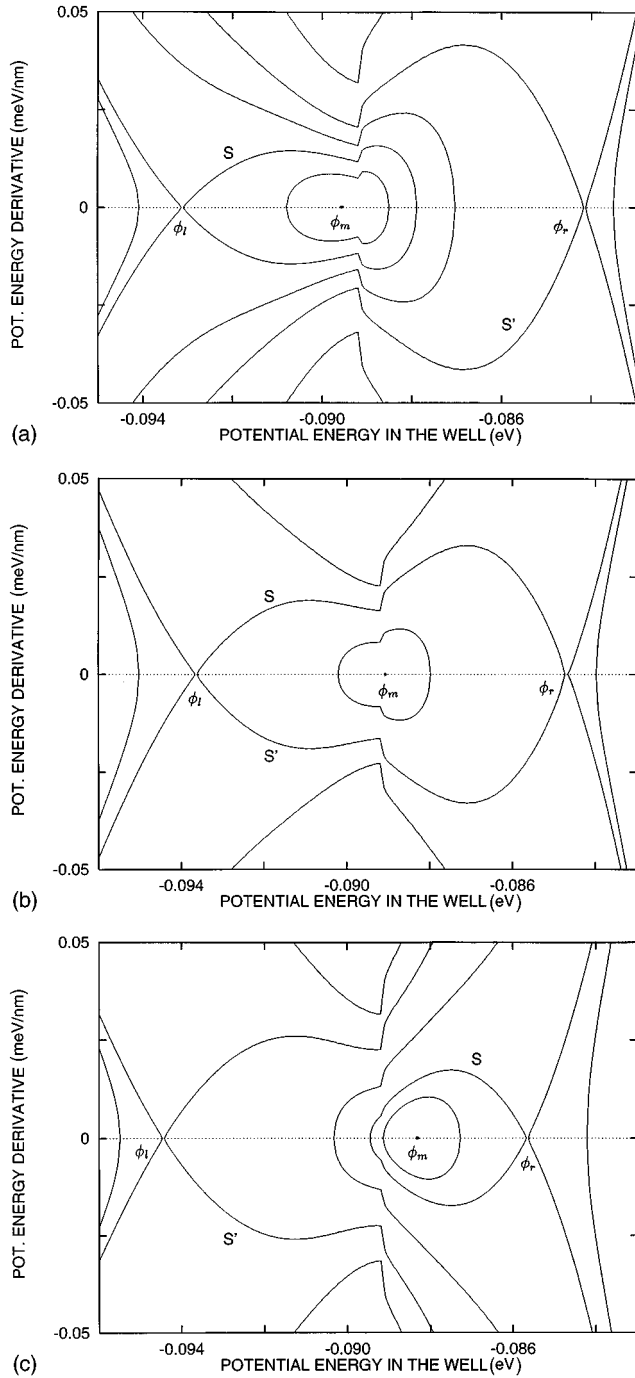
FIG. 6. Solutions of Eq. (18) on the phase plane $\phi - (d\phi/dy)$ for structure II at different voltages: (a) $\Phi = 0.244$ eV $< \Phi_c$, (b) $\Phi = 0.2475$ eV $= \Phi_c$, and (c) $\Phi = 0.246$ eV $> \Phi_c$.

The patterns shown in Fig. 7 can be interpreted in terms of the electron current. Actually, solitonlike and antisoliton-like patterns correspond to additional negative and positive built-up charges localized in finite domains of the quantum-well layer. The greater local electron concentration is due to the larger tunneling injection of electrons into the well, and, therefore, to larger local electric current. Thus the solitonlike patterns of Fig. 7(a) [the antisolitonlike patterns of Fig. 7(c)] means a local increase (decrease) in the electric current through the heterostructure, i.e., high (low) current strip layer. The kinklike pattern of Fig. 7(b) can be thought of as
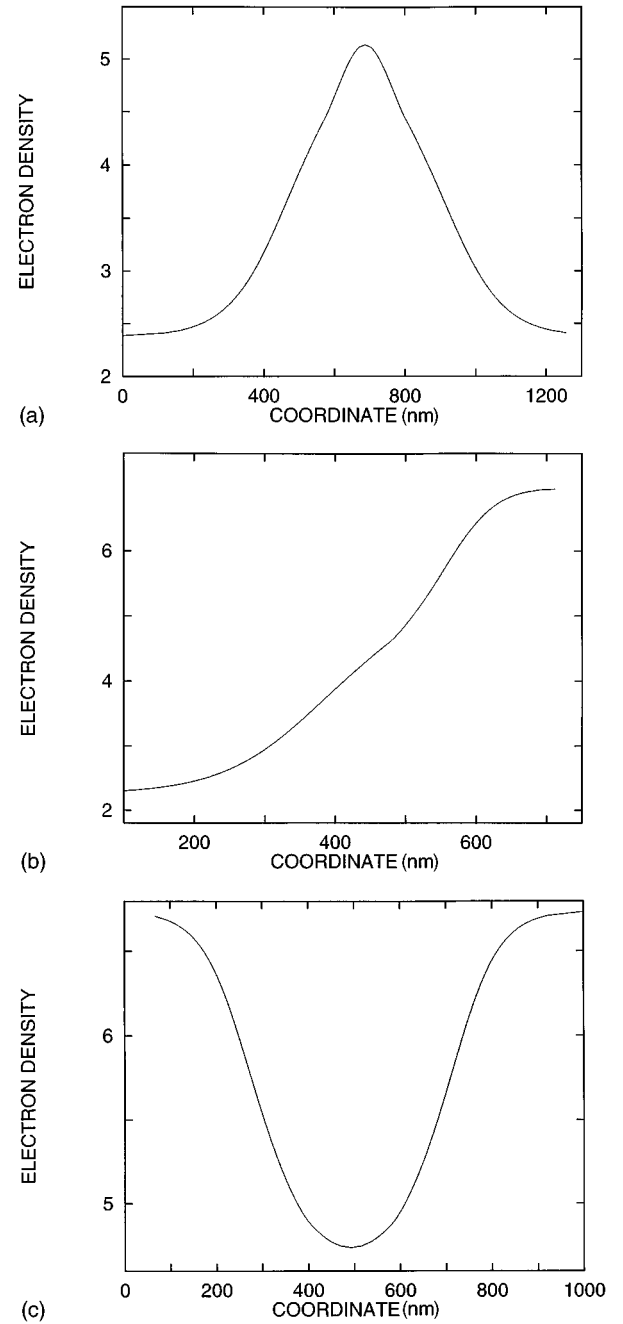


FIG. 7. Electron-density profiles (in units $10^{15}$ m$^{-2}$) for the patterns in structure II corresponding to phase portraits (a), (b), and (c) in Fig. 6.

a transient region between two uniform states with low and high built-up charges and currents. From the above-mentioned facts, can see that such a coexistence of the two states is possible only at certain bias $\Phi_c$.

Let us estimate the validity of the local approach. From Eq. (18) one can estimate the length scale of the patterns as

$$L_{st} \approx \left( \frac{\overline{\mathcal{D}} \overline{\tau}_{es}}{\delta} \right)^{1/2}, \qquad (22)$$

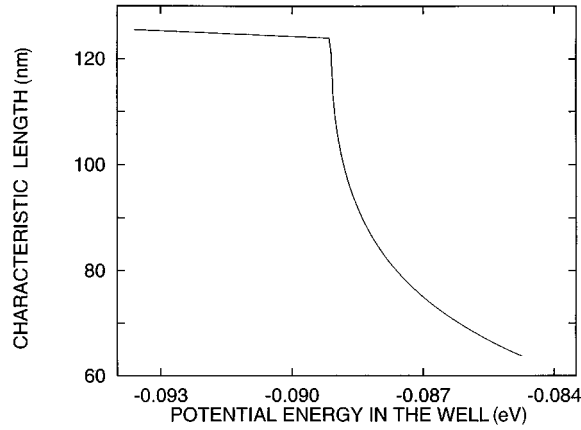where $\overline{\mathcal{D}}$ and $\overline{\tau}_{es}$ are average values, and

FIG. 8. The dependence of the characteristical length $L_{ch}$ on the potential energy $\phi$ in the quantum well for structure II.

$$\delta = \left| \frac{4\pi e^2}{\kappa} \frac{d_{B_1} d_{B_2}}{d} \frac{\overline{L} - \overline{R}}{\delta\phi} \right|.$$

Here $\overline{L}$ and $\overline{R}$ are average values of the left and right sides of Eq. (9), and $\delta\phi$ is a characteristical variation of $\phi$ within the pattern. As can be seen, $\sqrt{\overline{D}\overline{\tau}_{es}} \approx L_{ch}$ and the condition of validity of the local approach is $\delta \ll 1$. This condition can be realized in two cases: (a) for all voltages within the bistability range if the latter is small; and (b) for voltages corresponding to the edges of bistability for the arbitrary range $[\Phi_l, \Phi_h]$: nearby $\Phi_l$, it is valid for soliton types of solutions, nearby $\Phi_h$, for antisoliton types.

For the numerical examples of Fig. 7, the scale of the patterns is about 500–1000 nm. The dependence of $L_{ch}$ on $\phi$ for structure II is shown in Fig. 8. As can be seen, in this case the condition for validity of the local approach is satisfied.

## A. Solutions for finite transversal dimensions

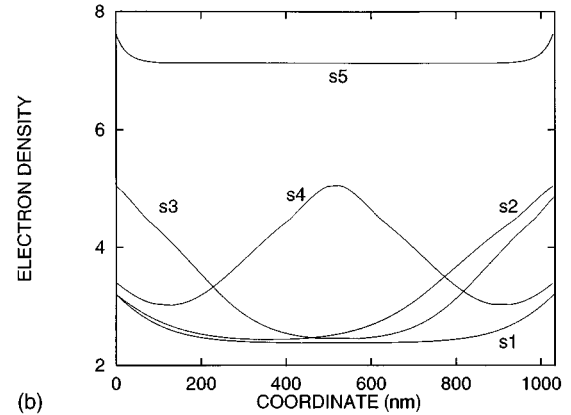For a heterostructure with finite transverse dimension,

$$-(L_y/2) < y < (L_y/2)$$

one should impose the boundary conditions that follow from Eq. (16):

$$-D(\phi)\frac{d\phi}{dy} = \pm S^{(\pm)}(\phi_e^\pm - \phi), \quad y = \pm \frac{L_y}{2} \qquad (23)$$

Boundary conditions can control possible patterns. In order to demonstrate this, let us combine Eqs. (23) with the phase portraits illustrated in Fig. 9(a). For simplicity, we assume that parameters $S^\pm$ and $\phi_e^{(\pm)}$ are independent of $\phi$. The boundary condition curves ($\pm 1$) are given for $S_1^{(+)} = S_1^{(-)} = 10^4$ m/s and $(Sn_e)_1^{(+)} = (Sn_e)_1^{(-)} = 1.5 \times 10^{20}$ m$^{-1}$ s$^{-1}$. The physical meaning of these constants is the following. If these boundary conditions are a result of some generation and recombination in the region near the sides of the structure with size, for example, $l_s = 10$ nm, then $S = 10^4$ m/s corresponds to the surface recombination time $\tau_s = l_s/S = 1$ ps, and the surface generation rate $Sn_e = 1.5 \times 10^{20}$ m$^{-1}$ s$^{-1}$ corresponds to production in this region of surface density $n_s = Sn_e\tau_s/l_s = 10^{16}$ m$^{-3}$ for the time $\tau_s$. The value of the ex-
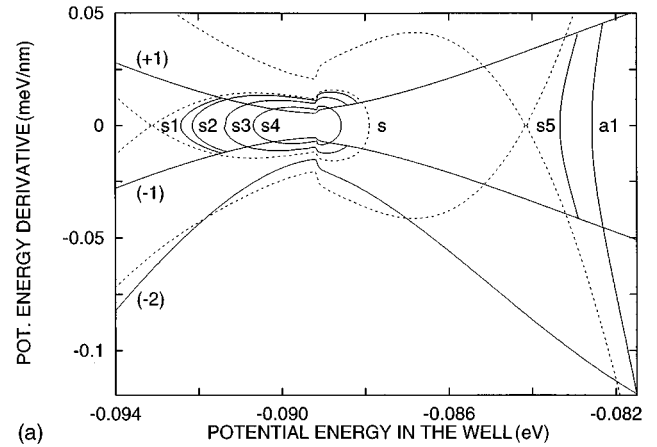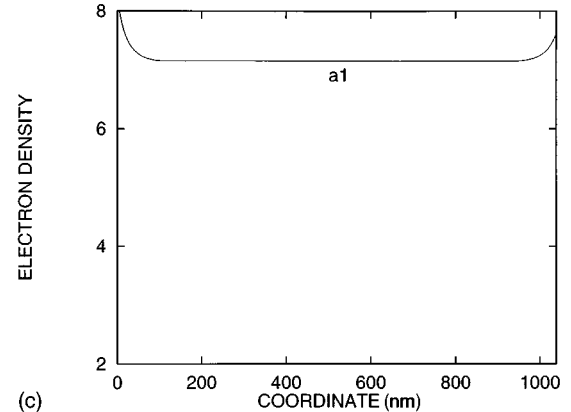






FIG. 9. (a) Boundary condition curves and possible phase trajectories (not in scale) for structure II with finite transverse dimensions. (b) Possible distributions of the electron density (in units $10^{15}$ m$^{-2}$). Calculations are performed for structure II with horizontal dimension $L_y = 1030$ nm. The edge conditions are symmetric and correspond to boundary condition curves ($\pm 1$) in (a). (c) The same for asymmetrical edge conditions, which correspond to boundary conditions curves ($+1$) and ($-2$) in (a).

ternal voltage is the same as for the phase portrait in Fig. 6(a). The trajectories, satisfying the boundary conditions, have to start at the ($-$) curve and end on the proper ($+$) curve. The direction of motion along the trajectory is determined by the condition that at positive $d\phi/dy$ the value $\phi$ increases during this motion, and vice versa. For given transversal dimensions one must select the trajectories for which

$$\int_{(-)}^{(+)} \left( \frac{d\phi}{dy} \right)^{-1} d\phi = L_y . \qquad (24)$$

The latter determines the integration constant in Eq. (19). For large enough $L_y$ and the symmetric boundary conditions $(-1)$ and $(+1)$ a number of different trajectories exist. For $L_y = 1030$ nm five of them are shown on the phase portrait in Fig. 9(a) (they are marked $s1$, $s2$, $s3$, $s4$, and $s5$). Corresponding coordinate dependences are depicted in Fig. 9(b).

Applying such an analysis, one can see that, if at least one of the edge generation rates $(Sn_e)^{(\pm)}$ is large, so that the proper boundary condition curve does not intersect the separatrix $s$, the patterns exist only at $\Phi > \Phi_c$. At $\Phi < \Phi_c$ only single state with high $\phi$ is to be realized. Curve $a1$ in Fig. 9(a) is shown for such a case for the parameters $S^{(-2)} = 3.5 \times 10^4$ m/s, $(Sn_e)^{(-2)} = 4.5 \times 10^{20}$ m$^{-1}$ s$^{-1}$ [the proper boundary condition curve $(-2)$ is presented in Fig. 9(a)]. This result means also that such a boundary condition conceals the low current branch of current-voltage characteristic of the whole device in the range $[\Phi_l, \Phi_c]$. Only one type of phase trajectory, $a1$, which corresponds to the profile with high electron and current densities, shown in Fig. 9(c), can exist. Analogously, one can show that if there is additional electron drain (recombination) on the boundaries, the high current branch is concealed in the range $[\Phi_c, \Phi_h]$. Strongly asymmetric boundary conditions, combining the above-mentioned ones at $y = \pm L_y/2$, conceal the multivaluedness. For the current-voltage characteristic this means the realization of a high current branch at $\Phi < \Phi_c$, and a low current branch at $\Phi > \Phi_c$. At a critical bias $\Phi = \Phi_c$ the current-voltage characteristic has a vertical portion. Obviously, each point of this vertical portion corresponds to the kinklike pattern, whose position determines the value of the current.

Varying $S^{(\pm)}$ and $(Sn_e)^{\pm}$, one can provide a number of different patterns, including periodical ones. As a result, we can conclude that the boundary conditions drastically affect patterns and allow the manipulation of the current-voltage characteristic.

### B. Nonstationary solutions

Above, we considered stationary patterns. In general, Eq. (14) allows different nonstationary solutions. The simplest of these are solutions in the form of autowaves, $\phi = \phi(\eta \equiv y - vt)$, where $v$ is the velocity of such a wave. For these autowave processes the additional term $-v(d\phi/dy)$ appears in Eq. (18). The usual analysis of the phase plane for the latter equation shows that, for a fixed bias $\Phi$ within the bistability range, there is a single velocity $v(\Phi)$, for which a solution in the form of a moving kink can exist. The solution can be thought of as a front, switching the system from one uniform state to another. At $\Phi = \Phi_c$ the velocity $v$ is zero, and we obtain a stationary kinklike solution, discussed above. In Fig. 10(a) the calculated $v(\Phi)$ is shown for structure II. The positive velocity corresponds to the autowave, switching the system from a high to a low current state.

### V. PATTERNS UNDER BALLISTIC REGIMES OF HORIZONTAL TRANSFER

Let us consider the range of parameters for which the local approach is not applicable. In particular, one should
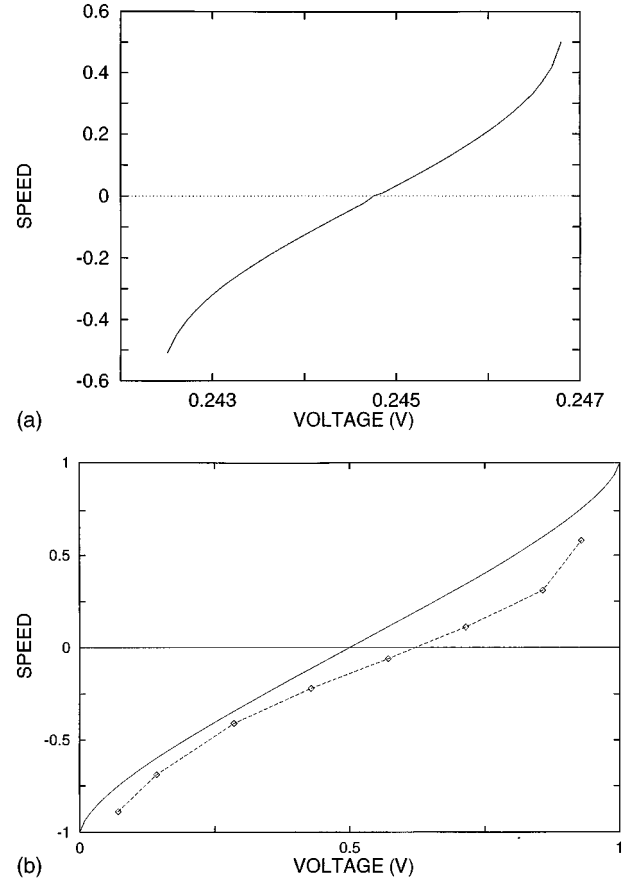


(a)

(b)

FIG. 10. (a) Velocity of switching wave (in units $v_F$) as a function of the voltage bias for structure II. (b) Dependences of switching wave velocity (in units $v_F$) on dimensionless voltage parameter $(\Phi - \Phi_l)/(\Phi_h - \Phi_l)$ for structure I. Solid line—results of calculations within the steplike model; dashed line—results of variational calculations.

work beyond the local approach if the resonant-tunneling structure demonstrates a wide range of bistability. For these cases one must analyze the kinetic equation (4) and algebraic equation (7). In the $\tau$ approximation the collision integral can be approximated as $I\{f\} \approx -f_1/\tau_{sc}$, where $f_1$ is asymmetrical part of distribution function $[f_1(y,p) = -f_1(y,-p)]$, and $\tau_{sc}$ is the scattering time. We are going to consider the case of ballistic electron horizontal transfer, which takes place if $\tau_{sc} \gg \tau_{es}$. As shown in Sec. III, the wide bistability range can be realized if $\tau_{ew}$ is smaller then $\tau_{sc}$ and $\tau_{cw}$. This proves that, in structures with wide bistability, horizontal electron transfer can be ballistic. In this case the kinetic equation is

$$\frac{\partial f}{\partial t} + \frac{p}{m^*} \frac{\partial f}{\partial y} - \frac{\partial \phi}{\partial y} \frac{\partial f}{\partial p} = G - \frac{f}{\tau_{es}} . \qquad (25)$$

Here $p$ labels the $y$ component of momentum $\mathbf{p}$. One can solve Eq. (25) in terms of the characteristic curves

$$p = \pm \sqrt{p_0^2 + 2m^*[\phi(y_0) - \phi(y)]} \equiv \mathcal{P}(p_0, y_0, y), \quad (26)$$

where $p_0$ is the momentum of the electron, injected into the well at the point $y = y_0$. The general solution of the kinetic equation has the form

$$f(y,p) = \int m^* \frac{dy'}{\mathcal{P}(p,y,y')} M(p,y,y') G[\mathcal{P}(p,y,y'),y'], \tag{27}$$

where the kernel $M(p,y,y')$ depends on the particular shape of the potential $\phi(y)$ and the boundary conditions. Results of calculations of $M$ are presented in Appendix D.

Using Eqs. (27), (5), and (7), one can obtain the following integral equation for $\phi$:

$$\phi = -\frac{d_{B_1}}{d} \Phi + \frac{4\pi e^2 d_{B_1} d_{B_2}}{\kappa d} m^* \sum_p \int \frac{dy'}{\mathcal{P}} MG. \tag{28}$$

This nonlinear integral equation takes place of partial differential equation (4) and relationship (7).

Nonlinear integral equation (28) is too complex to be solved analytically. Moreover, there is no general approach for a numerical solution. We analyzed the problem of patterns, introducing two simplifications into Eq. (25). First, we assume the steplike character of $G$ and $\tau_{es}$ as functions of $\phi$:

$$G = \begin{cases} 0, & \varepsilon_0 + \phi < 0 \\ \dfrac{1}{\tau^{(h)}} F\left(\dfrac{p^2}{2m^*}\right), & \varepsilon_0 + \phi > 0, \end{cases} \tag{29}$$

$$\tau_{es} = \begin{cases} \tau^{(l)}, & \varepsilon_0 + \phi < 0 \\ \tau^{(h)}, & \varepsilon_0 + \phi > 0, \end{cases} \tag{30}$$

where $F$ is the Fermi function (see Appendix A). This means that we assume that electron tunnel injection from the emitter to the well (EW) takes place only if the resonant level lies above the bottom of emitter band and the rate of injection in this case does not depend on the position of the resonant level. Second, in Eq. (25), we neglect by a term, proportional to the force (i.e., we consider the horizontal transfer as free motion of electrons). These assumptions are valid if a variation of $\phi$ within the pattern is smaller then $E_F$: under this condition (i) the population of states in the emitter, which are in resonance with a quasibound state, is almost constant within the pattern; and (ii) the kinetic energy of electrons is large with respect to their potential energy.

Within the described model the only parameters of the potential profile which affect the solution of the kinetic equation are the positions of the boundaries of the injection region, where $\varepsilon_0 + \phi > 0$ (i.e., where tunnel injection from the emitter exists). This allows us to solve the problem of patterns. Qualitatively, we obtained the same results as for the case of weak bistability in the local approach. The critical voltage at which the kinklike pattern exists corresponds to the center of the bistability region: $\Phi_c = (\Phi_l + \Phi_h)/2$. At $\Phi_l < \Phi < \Phi_c$ a solitonlike pattern is possible, while at $\Phi_c < \Phi < \Phi_h$ an antisolitonlike pattern can be realized. At $T = 0$ the width of soliton $L_s$ (the width of the injection region) is determined by the equation

$$2\frac{\Phi - \Phi_l}{\Phi_h - \Phi_l} = 1 - \mathcal{F}\left(\frac{L_s}{v_F \tau^{(h)}}\right), \tag{31}$$

and the width of antisoliton $L_a$ (width of the region with no injection) is determined by the equation

$$2\frac{\Phi - \Phi_l}{\Phi_h - \Phi_l} = 1 + \mathcal{F}\left(\frac{L_a}{v_F \tau^{(l)}}\right), \tag{32}$$

where

$$\mathcal{F}(x) = \frac{4}{\pi} \int_0^1 \sqrt{1 - z^2} \, \exp\left(-\frac{x}{z}\right) dz.$$

Autowave patterns exist as well. Their speed $v$ is determined by the equation

$$\frac{\Phi - \Phi_l}{\Phi_h - \Phi_l} = 1 - \frac{1}{\pi}\left[\frac{\pi}{2} - \frac{v}{v_F}\left(1 - \frac{v^2}{v_F^2}\right)^{1/2} - \arcsin\frac{v}{v_F}\right]. \tag{33}$$

In Fig. 10(c) the dependence of $v/v_F$ on the voltage parameter $(\Phi - \Phi_l)/(\Phi_h - \Phi_l)$ is shown by the solid line.

In order to obtain results without the above-mentioned assumptions, we applied the following variational procedure for the solution of self-consistent integral equation (28). Let us introduce the functional

$$J\{\phi\} = \int dy |\phi - \mathcal{L}\{\phi\}| \tag{34}$$

where

$$\mathcal{L}\{\phi\} = -\frac{d_{B_1}}{d} \Phi + \frac{4\pi e^2 d_{B_1} d_{B_2}}{\kappa d} m^* \sum_p \int \frac{dy'}{\mathcal{P}} MG. \tag{35}$$

Functional $J$ equals zero for the exact solution of Eq. (28). For a particular solution we can choose some probe functions $\phi_{pr}(y,c_i)$, where $c_i$ are variational parameters. These parameters are determined by the condition of minimization of $J(c_i)$.

Using this method, we analyzed all three types of basic solutions: soliton, antisoliton, and kinklike. Here we present the switching kinklike autowaves in the case of ballistic electron transfer. As in this case we deal with a nonstationary kinetic equation one must introduce an additional shift $m^* v$ in the momentum dependence of $G$ in Eq. (27). Applying different probe functions, we found that the best fit corresponds to an arctanlike spatial dependence of $\phi$:

$$\phi_{pr} = \tfrac{1}{2}(\phi_l + \phi_r) + \frac{1}{\pi}(\phi_r - \phi_l)\arctan(\gamma y), \tag{36}$$

where $\phi_l$ and $\phi_h$ are the potential energies in the well, corresponding to the low and high charge density uniform states. This kind of probe function has two parameters: $\gamma$ and the switching velocity $v$. The dependence of $v/v_F$ on the dimensionless voltage $(\Phi - \Phi_l)/E_F$ for structure I is shown in Fig. 9(b). As discussed in Sec. IV B, the positive velocity means switching from a high-current state. One can see that the latter result is in an agreement with approximation of Eq. (33).

In the case of the wide range of bistability and ballistic horizontal electron transfer the spatial scale of the patterns is of the order of $L_{ch}$. The strong dependence of the tunneling injection rate on the position of the resonant level and the ballistic motion of electrons in the quantum well lead to a considerable spatial broadening of the collector current den-
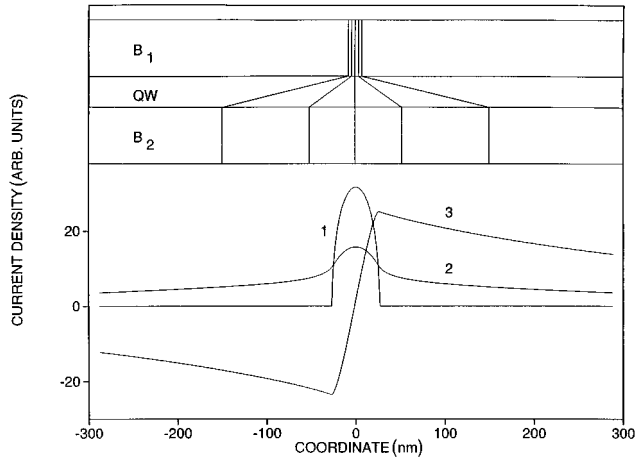
FIG. 11. The spatial dependence of the current for the soliton-like pattern. In the upper part the current field is depicted. In the lower part the emitter (curve 1), collector (curve 2, multiplied by factor 5), and two-dimensional lateral (curve 3) currents are presented. Calculations are done for structure I. The voltage bias corresponds to the condition $(\Phi-\Phi_l)/(\Phi_h-\Phi_l)=0.3$.

sity with respect to the emitter current density. In Fig. 11, spatial dependences of emitter, collector, and two-dimensional lateral current densities are shown for the solitonlike pattern in structure $I$ at $(\Phi-\Phi_l)/(\Phi_h-\Phi_l)=0.3$. In the upper part of Fig. 11 the current field in the structure is shown (the spacing between the current lines is proportional to the value of current density). The current field in the quantum-well layer is presented conditionally. In the lower part of Fig. 11 all three currents are plotted. One can see considerable current leakage over the quantum well.

## VI. DISCUSSION

Different layered heterostructures with the resonant-tunneling mechanism of the carrier transport frequently demonstrate a bistable behavior of the tunneling current. The physical reason for the intrinsic bistability is the dynamic buildup of the electric charge, which leads to two possible positions of the quasibound state in the quantum well: low and high currents at the same voltage bias. In general, the electric charge can build up in the quantum well between the barriers, in the emitter spacer notch before the barriers, in barrier layers (for heterostructures of type II), etc. As a result a variety of current-voltage characteristics with the intrinsic bistability is observed: a $Z$ type,[12–14] an $S$ type,[28] more complex butterflylike,[29] etc.

The bistable effects attract attention, are well understood, and are described by different *one-dimensional* theories. In the framework of such one-dimensional approaches only carrier motion perpendicular to heterojunctions is taken into account, and parallel (lateral) carrier transfer is disregarded. Meanwhile, lateral carrier transfer exists in layered structures and is of importance under bistable effects. The lateral transfer brings about the simultaneous coexistence of different possible states of the system, i.e., the formation of self-sustained spatially nonuniform distributions of the built-up charge, resonant current, etc. The formation of patterns is well known in macroscopic solid-state physics, but bistable

resonant tunneling systems provide an example with the quantum character of the carrier motion at least in one (perpendicular) direction.

In this paper we developed an approach which allows us to consider the tunneling in a double-barrier structure, to take into account self-consistently the nonuniform built-up charge and lateral carrier transfer. We obtained that the patterns in question are characterized by a lateral scale exceeding the thickness of the structure (in the perpendicular direction) considerably. The scale of the patterns $L_{ch}$ is determined by the time of electron escape from the well and the Fermi velocity of electrons in the emitter ($L_{ch}=v_F\tau_{es}$). This is a result of the ballistic (or quasiballistic) character of electron horizontal transfer. The shape of the patterns depends on the applied bias, and can be of soliton, antisoliton, and kinklike forms.

For heterostructures with finite dimensions of the layers, the patterns can be more complicated. Conditions on the edges of the heterostructure should be involved in consideration. The approach developed allowed us to consider different edge conditions. We showed that the number of patterns and their properties are strongly influenced by these conditions. In particular, these edge conditions can cancel some branches of the current-voltage characteristic corresponding to low or high current through the entire structure. In this context, we point out that, despite a vast number of papers on resonant tunneling, only a few paid attention to the edge effects on the tunneling current.[18,30] Our analysis showed that lateral transfer has a large characteristic scale, and the decrease in lateral dimensions of resonant structures should certainly lead to size effects in the resonant tunneling. It is worth mentioning that the effect of horizontal electron leakage can be important even if the structure does not possess bistable behavior.[18,30]

Besides stationary patterns, mobile patterns have been found. In particular, we described patterns which produce a switching of the heterostructure from one uniform current state to the another. The velocity of such switching waves depends on voltage and is of the order of the Fermi velocity $v_F$.

Let us briefly discuss the problem of stability of stationary patterns. This is an important question since it determines the possibility of pattern observation in the experiments. It requires special investigation. Here we restrict ourselves to a short discussion of this problem in the case of weak bistability patterns described by Eq. (14). Equations of this type often appear in different problems of self-organization (see, for example, Ref. 21). Stability problem of such patterns against small perturbations can be formulated mathematically in terms of the Sturm-Liouville eigenvalue problem. For infinite dimensions the result is that soliton and antisoliton patterns are unstable, while a kinklike pattern is stable. If the system under consideration has some *imperfections or defects*, all three basic solutions can be stabilized by pinning on defects.

Uniform solutions are stable against small perturbations. However, the soliton and antisoliton patterns are those which inspire the propagation of switching waves, described in Sec. IV B. That is, uniform high and low current states are unstable with respect to *strong* perturbations. That is, the low (high) current uniform state at $\Phi_l<\Phi<\Phi_c$ ($\Phi_c<\Phi<\Phi_h$)

can be switched to the high (low) current uniform state by means of strong enough perturbation of built-in charge, localized in a finite spatial region.

For finite lateral dimensions of the structure, the situation is more complicated, and stability strongly depends on the boundary conditions at the edges of the heterostructure and the lateral dimensions. In particular, for fixed values of the electron density at the edges of the quantum-well layer, patterns can be stable.[21] It is worth adding that the stability of the patterns can also depend on the properties of the external circuit in which the resonant-tunneling diode is included.

In conclusion, we studied the effect of the pattern formation in double-barrier resonant-tunneling heterostructures with an intrinsic bistability of the current-voltage characteristic. The effect considerably involves the lateral carrier transport, and exists for both coherent and sequential mechanisms of the resonant tunneling. The patterns are characterized by an alternative position of the resonant level in the quantum well, a nonuniform distribution of resonant electrons in the quantum-well layer, and a nonuniform tunneling current density through the heterostructure.

### APPENDIX A: EQUATION FOR HORIZONTAL ELECTRON TRANSFER

In electrodes, electrons can be characterized by the $z$ projection of the momentum $p_z$ (or corresponding energy of vertical motion $\varepsilon$) and lateral momentum $\mathbf{p}=\{p_x,p_y\}$. The distribution functions are supposed to be the Fermi functions $F(E-E_F)$:

$$f^{(e)}(\mathbf{p},p_z)=F\left(\frac{p^2+p_z^2}{2m^*}-E_F\right),$$

$$f^{(c)}(\mathbf{p},p_z)=F\left(\frac{p^2+p_z^2}{2m^*}+\Phi-E_F\right). \qquad (A1)$$

For classical motion along the well, one can introduce the distribution function $f(\mathbf{r},\mathbf{p},t)$, which depends on two-dimensional vectors, $\mathbf{r}=\{x,y\}$ and $\mathbf{p}$. We assume that the transversal coordinate dependence of patterns is so smooth that the tunneling can be accounted as strictly vertical process (along $z$ at fixed $\mathbf{r}$. Then, in terms of tunneling transitions between the emitter, quantum well, and collector (EW, CW), the total derivative of $f(\mathbf{r},\mathbf{p},t)$ can be written as[31]

$$\frac{df}{dt}=\sum_{\mathbf{p}',p_z} W^{(ew)}_{\mathbf{p}',p_z;\mathbf{p},\varepsilon_0}[f^{(e)}(\mathbf{p}',p_z)-f(\mathbf{r},\mathbf{p})]$$

$$+\sum_{\mathbf{p}',p_z} W^{(cw)}_{\mathbf{p}',p_z;\mathbf{p},\varepsilon_0}[f^{(c)}(\mathbf{p}',p_z)-f(\mathbf{r},\mathbf{p})]+I\{f\},$$

$$(A2)$$

where the first and second terms on the right-hand side are the rates of tunneling between the emitter and the well and between the well and collector, respectively. The probabilities of tunneling $W^{(ew)}$ and $W^{(cw)}$ generally depend on the electron scattering. The last term in Eq. (A2) describes changes in the distribution function due to scattering of electrons during their quasiclassical motion along the well. If we neglect broadening of the quasibound level and assume the conservation of the electron lateral momentum upon tunneling, it is possible to write

$$W^{ew}_{\mathbf{p}',p_z;\mathbf{p},\varepsilon_0}=w^{ew}(\varepsilon_0)\,\delta_{\mathbf{p}',\mathbf{p}}\delta_{p_z,\pm p_0},\quad p_0=\sqrt{2m^*(\varepsilon_0+\phi)},$$
$$(A3)$$

$$W^{cw}_{\mathbf{p}',p_z;\mathbf{p},\varepsilon_0}=w^{cw}(\varepsilon_0-\Phi)\,\delta_{\mathbf{p}',\mathbf{p}}\delta_{p_z,\pm p_1},$$

$$p_1=\sqrt{2m^*(\varepsilon_0+\phi+\Phi)}, \qquad (A4)$$

where $w^{ew}$ and $w^{cw}$ are the probabilities of one dimensional tunneling through the emitter and collector barriers for the electron energies $\varepsilon_0+\phi$ and $\varepsilon_0+\phi+\Phi$, respectively. For Eq. (A3) the signs ($\pm$) correspond to the transitions $E\leftrightarrows W$. For Eq. (A4) the signs ($\pm$) correspond to the transitions $W\leftrightarrows C$. The coefficients $w^{ew}$ and $w^{cw}$ do not depend on the momenta $\mathbf{p}$, but they are, in general, functions of the potential profile of biased heterostructure; $\phi$ is the electrostatic potential energy in the well.

In order to calculate $w^{ew}$ and $w^{cw}$, we define the energy of the resonant level as follows. Since in our model we assume a narrow quantum well, the position of the resonant level with respect to the well bottom is, mainly, determined by the width and depth of the well. Finite thicknesses of the barriers cause small corrections to this value. Let $\varepsilon_0^{(\infty)}$ be the position of the level if we neglect finite transmission coefficients of the barrier. Then, the true resonant energy as a function of the bias $\Phi$ can be written as

$$\varepsilon_0(\phi)=\varepsilon_0^{(\infty)}+\Delta\{1-[\,\delta(\varepsilon_0^{(\infty)},\phi,\Phi)]^2\} \qquad (A4')$$

where $\Delta=V+\phi-\varepsilon_0^{(\infty)}$, and

$$\delta(\varepsilon,\phi,\Phi)=1+\left[1-2\frac{\Phi+\varepsilon}{V}\right]e^{-2\beta}+\left[1-2\frac{\varepsilon}{V}\right]e^{-2\alpha},$$

$$\alpha(\varepsilon)=\frac{2}{3}\left(\frac{2m^*}{\hbar^2}\right)^{1/2}\frac{d_{B_1}}{\phi}\,[\,\sqrt{(V+\phi-\varepsilon)^3}-\sqrt{(V-\varepsilon)^3}\,],$$

$$(A4'')$$

$$\beta(\varepsilon)=\frac{2}{3}\left(\frac{2m^*}{\hbar^2}\right)^{1/2}\frac{d_{B_2}}{\phi+\Phi}\,[\,\sqrt{(V+\phi-\varepsilon)^3}$$

$$-\sqrt{(V-\Phi-\varepsilon)^3}\,].$$

For $w^{(ew)}$ and $w^{(cw)}$, we obtain

$$w^{(ew)}=\frac{8}{\hbar}\frac{\Delta}{V}\,\sqrt{\varepsilon_0(\phi)[V-\varepsilon_0(\phi)]}e^{-2\alpha[\varepsilon_0(\phi)]},$$

$$w^{(cw)}=\frac{8}{\hbar}\frac{\Delta}{V}\,\sqrt{[\Phi+\varepsilon_0(\phi)][V-\Phi-\varepsilon_0(\phi)]}e^{-2\beta[\varepsilon_0(\phi)]}.$$

Assuming a strong voltage bias, we can neglect tunneling from the collector to the well and rewrite Eq. (A2):

$$\frac{df}{dt} = \frac{1}{\tau_{\text{ew}}} \Theta(\varepsilon_0 + \phi) F\left(\frac{p^2}{2m^*} + \varepsilon_0 + \phi - E_F\right) - \frac{f}{\tau_{\text{es}}} + I\{f\}$$

$$\equiv G(\mathbf{p}, \phi) - \frac{f}{\tau_{\text{es}}} + I\{f\}. \tag{A5}$$

Here $\Theta$ is the Heaviside function, and we introduce the local rate of tunneling injection of the electrons into the well layer:

$$G(\mathbf{p}, \phi) = \frac{1}{\tau_{\text{ew}}} \Theta(\varepsilon_0 + \phi) F\left(\frac{p^2}{2m^*} + \varepsilon_0 + \phi - E_F\right), \tag{A6}$$

and $\tau_{\text{ew}} \equiv 1/w^{(\text{ew})}$, $\tau_{\text{cw}} \equiv 1/w^{(\text{cw})}$, and $\tau_{\text{es}} \equiv 1/(w^{(\text{ew})} + w^{(\text{cw})})$.

Formulas (A3)–(A6) are valid for the limit of zero width of the quasibound level. Broadening of this level can be important for the voltage bias, aligning the level and the bottom of the emitter band. Two processes lead to the broadening: finite transmission of the barriers and scattering in the quantum well. We assume density of states, associated with the level in the form

$$\rho(\varepsilon, \varepsilon_0) = \frac{1}{\pi} \frac{\Gamma}{(\varepsilon - \varepsilon_0 - \phi)^2 + \Gamma^2}, \tag{A6$'$}$$

where $\varepsilon$ is energy of vertical motion, and $\Gamma$ is the broadening of the level. Two above-mentioned processes contribute to the broadening: $\Gamma = \hbar(1/\tau_{\text{es}} + 1/\tau_{\text{sc}})/2$, where $\tau_{\text{sc}}$ is the scattering time for the electrons in the well. Equation ($A6'$) is valid for weak broadening: $\Gamma \ll \varepsilon_0$ (see Ref. 32). Taking the broadening into account, one can modify the kinetic equation (A5) as follows. In Eq. (A6), for the injection rate one should substitute

$$\Theta(\varepsilon_0 + \phi) \to \nu(\varepsilon_0 + \phi) = \int_0^\infty d\varepsilon \; \rho(\varepsilon, \varepsilon_0 + \phi). \tag{A6$''$}$$

Of course, in this case one should put $\varepsilon_0 + \phi = E_F$ in the argument of the Fermi function in Eq. (A6).

This modification of $G(\mathbf{p}, \phi)$ is important for biases near the edge of the bistability region for any broadening, and it should be included into consideration at all biases if the bistable region is narrow. Writing the total derivative $df/dt$ in Eq. (A5) in an explicit form, we obtain the basic kinetic equation (4).

## APPENDIX B: ONE-DIMENSIONAL APPROXIMATION FOR ELECTROSTATIC ENERGY

The Poisson equation $\Delta\varphi = -(4\pi e^2/\kappa) n(x,y,z)$ under boundary conditions (3) has the solution

$$\varphi(x,y,z) = -\Phi \frac{z}{d} - \frac{4\pi e^2}{\kappa} \int dx' dy' dz' \mathcal{G}(x-x', y$$
$$- y', z, z') n(x', y', z'), \tag{B1}$$

where $\mathcal{G}$ is the Green function with the boundary conditions $\mathcal{G}|_{z=0} = \mathcal{G}|_{z=d} = 0$. To satisfy these conditions, we present $\mathcal{G}$ as a series:

$$\mathcal{G}(x-x', y-y', z, z') = \sum_k \; \sin\frac{\pi k(z + d_{B_1})}{d}$$
$$\times F_k(x-x', y-y', z'). \tag{B2}$$

For $F_k$, one can find

$$F_k(x,y,z') = -\frac{1}{\pi d} \sin\frac{\pi k(z' + d_{B_1})}{d} K_0\left(\frac{\pi k}{d} \sqrt{x^2+y^2}\right), \tag{B3}$$

where $K_0$ is the McDonald function. For the electrostatic energy in the well, $\varphi(x,y,d_{B_1}) \equiv \phi(x,y)$, we obtain Eq. (6) with the kernel function

$$K(\mathbf{r}-\mathbf{r}') = \frac{4e^2}{\kappa d} \sum_k \; \sin^2\left(\frac{\pi k d_{B_1}}{d}\right) K_0\left(\frac{\pi k}{d} |\mathbf{r}-\mathbf{r}'|\right). \tag{B4}$$

For the patterns, depending on the one transversal coordinate, say $y$, only the integral on $y'$ remains in Eq. (6). In this case the kernel function is

$$K(y-y') = \frac{4e^2}{\kappa} \sum_k \; \sin^2\left(\frac{\pi k d_{B_1}}{d}\right) e^{-\pi k|y-y'|/d}. \tag{B5}$$

From Eqs. (B4) and (B5), it follows that the kernel function exponentially decays for the argument, exceeding the thickness of the structure $d$. For the smooth dependences $n(x,y)$ this proves the one-dimensional consideration of the electrostatic problem employed in Eq. (7).

## APPENDIX C: LOCAL APPROACH FOR HORIZONTAL TRANSFER

Integrating kinetic equation (4) over $\mathbf{p}$, one can easily obtain the balance equation for horizontal transport:

$$\frac{\partial n}{\partial t} + \text{div}\mathbf{j} = g[\phi(\mathbf{r},t)] - \frac{n}{\tau_{\text{es}}}, \tag{C1}$$

where we introduce the two-dimensional electron flux

$$\mathbf{J} = \sum_{\mathbf{p}} \; \frac{\mathbf{p}}{m^*} f(\mathbf{r}, \mathbf{p}) \tag{C2}$$

and total injection rate

$$g = \frac{\nu(\varepsilon_0 + \phi)}{\tau_{\text{ew}}(\phi)} \sum_{\mathbf{p}} \; F\left(\frac{p^2}{2m^*} + \varepsilon_0 + \phi - E_F\right). \tag{C3}$$

From the theory of electron transport it is well known that an equation in form of Eq. (C1) can be significantly simplified for the case where a *local approximation* is applicable i.e., current (C2) can be expressed through the concentration $n$, the potential $\phi$, and their derivatives. For this the length and time scales of the problem should be sufficiently greater than the relaxation length and time of the electron momentum (see, for example, Ref. 33). Such a hierarchy of the characteristic scales provides an almost symmetric distribution function in the momentum space. The analysis given in Sec. III showed that, for bistable regimes, momentum relaxation is not the fastest process, and can be completely absent. This

means, that electron distribution relaxation occurs mainly as a result of tunneling exchange between the quantum well and the electrodes. This exchange can lead to an almost symmetric distribution function even if the momentum relaxation is negligible. The standard approach cannot be used in the case in question. We introduce the local approximation in another way. Supposing that the potential $\phi(\mathbf{r},t)$ is given, we find the concentration $n(\mathbf{r},t)$ through $\phi$ and its derivatives on $\mathbf{r}$ and $t$. Then, this result and relationship (7) will compose the self-consistent system of equations which will describe the patterns in the local approximation.

In order to derive the equation for $n = n[\phi,(\partial\phi/\partial r),(\partial^2\phi/\partial r^2),(\partial\phi/\partial t),\dots]$ in the local approximation, it is convenient to present the distribution function as $f(\mathbf{r},\mathbf{p},t)=f^{(+)}(\mathbf{r},\mathbf{p},t)+f^{(-)}(\mathbf{r},\mathbf{p},t)$, where $f^{(+)}(\mathbf{r},\mathbf{p},t)=f^{(+)}(\mathbf{r},-\mathbf{p},t)$ is symmetric, while $f^{(-)}(\mathbf{r},\mathbf{p},t)=-f^{(-)}(\mathbf{r},-\mathbf{p},t)$ is an asymmetric function of $\mathbf{p}$. Since the injection rate $G$ is symmetric, we obtain the coupled equations

$$\frac{\partial f^{(+)}}{\partial t}+\frac{\mathbf{p}}{m^*}\frac{\partial f^{(-)}}{\partial \mathbf{r}}-\frac{\partial\phi}{\partial\mathbf{p}}\frac{\partial f^{(-)}}{\partial\mathbf{p}}=G-\frac{f^{(+)}}{\tau_{es}}, \quad (C4)$$

$$\frac{\partial f^{(-)}}{\partial t}+\frac{\mathbf{p}}{m^*}\frac{\partial f^{(+)}}{\partial \mathbf{r}}-\frac{\partial\phi}{\partial\mathbf{p}}\frac{\partial f^{(+)}}{\partial\mathbf{p}}=-\frac{f^{(-)}}{\tau_{es}}-\frac{f^{(-)}}{\tau_{sc}}, \quad (C5)$$

where we suppose elastic scattering inside the well, and write the collision integral in the $\tau$ approach with momentum independent scattering time $\tau_{sc}$. Then we assume a smoothness of the patterns and a gradient expansion of all functions. To trace the derivation we formally introduce two dimensionless parameters $\theta_1$ and $\theta_2$ by the following replacements: $(\partial/\partial t)\rightarrow\theta_1(\partial/\partial t)$, $(\partial/\partial\mathbf{r})\rightarrow\theta_2(\partial/\partial\mathbf{r})$ (in the final formulas we set $\theta_1=\theta_2=1$). Then all functions can be presented as expansions in series with respect to $\theta_1$ and $\theta_2$:

$$f^{(+)}=f^{(+)}_{00}+\theta_1 f^{(+)}_{10}+\theta_2^2 f^{(+)}_{02}+\cdots,$$

$$f^{(-)}=\theta_2 f^{(-)}_{01}+\theta_1\theta_2 f^{(-)}_{11}+\theta_2^3 f^{(-)}_{03}+\cdots,$$

$$n=n_0+\theta_1 n_{10}+\theta_2^2 n_{02}+\cdots, \quad (C6)$$

$$\mathbf{J}=\theta_2\mathbf{J}_{01}+\theta_1\theta_2\mathbf{J}_{11}+\theta_2^3\mathbf{J}_{03}+\cdots,$$

Thus the terms proportional to $\theta_1^{s_1}\theta_2^{s_2}$ contain the $s_1$th power of the time derivative and the $s_2$th power of the gradient; from Eqs. (C4) and (C5) we easily find the lowest approximations.

$$f^{(+)}_{00}[(\mathbf{r}),\mathbf{p},t]=\tau_{es}G(\mathbf{r},\mathbf{p}), \quad (C7)$$

$$f^{(-)}_{01}(\mathbf{r},\mathbf{p},t)=\tau_{eff}\left\{\frac{p}{m^*}\frac{\partial f^{(+)}}{\partial\mathbf{r}}-\frac{\partial\phi}{\partial\mathbf{p}}\right\}, \quad (C8)$$

$$n_0=\tau_{es}(\phi)g(\phi), \quad (C9)$$

$$\mathbf{J}_{01}=-\left[\frac{\tau_{eff}n_0}{m^*}+\frac{d}{d\phi}\left(\frac{2\tau_{eff}n_0\langle\varepsilon\rangle}{m^*}\right)\right]\frac{\partial\phi}{\partial\mathbf{r}}\equiv-D(\phi)\frac{\partial\phi}{\partial\mathbf{r}}, \quad (C10)$$

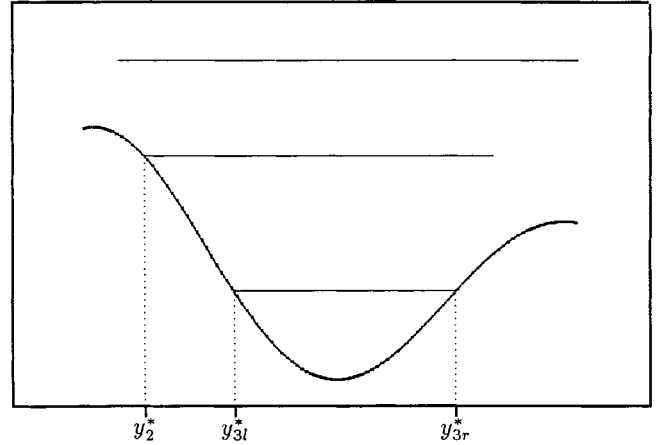where $1/\tau_{eff}=1/\tau_{es}+1/\tau_{sc}$, and $\langle\varepsilon\rangle$ is average electron kinetic energy:



FIG. 12. Model potential profile illustrating three possible types of trajectories of ballistic electrons injected in the quantum well.

$$\langle\varepsilon\rangle=\frac{\int d\mathbf{p}\frac{p^2}{2m^*}f_{00}}{n_0} \quad (C11)$$

Now we can write the corrections of high orders for $n$:

$$n_{10}=-\tau_{es}\frac{\partial n_0}{\partial t}, \quad n_{02}=-\tau_{es}\mathrm{div}\mathbf{J}_{01}. \quad (C12)$$

We restrict ourselves to the three-term approximation of $n$ given by Eq. (C6). Then we find $n$ in the form

$$n\left(\phi,\frac{\partial^2\phi}{\partial\mathbf{r}^2},\frac{\partial\phi}{\partial t}\right)=n_0(\phi)-\tau_{es}(\phi)\frac{\partial n_0}{\partial t}-\tau_{es}(\phi)$$
$$+\mathrm{div}\left(D(\phi)\frac{\partial\phi}{\partial\mathbf{r}}\right), \quad (C13)$$

where we set $\theta_1=\theta_2=1$. Combining formula (C13) and relationship (7), one can obtain the equation for $\phi(\mathbf{r},t)$.

In the above derivation we neglect the terms with derivatives of the higher order. This is valid only for the patterns with smooth time and coordinate dependences [see criteria (17)].

## APPENDIX D: KERNELS FOR INTEGRAL EQUATION (27)

The model fragment of potential $\phi(y)$ in Fig. 12 illustrates three possible cases for injected electrons. If an electron is injected with lateral motion energy, exceeding a maximum of $\phi(y)[p^2/(2m^*)+\phi(y_0)>\max\phi(y)]$, no turning points exist, and

$$M(p_0,y_0,y)=\Theta(y-y_0)e^{-h(p_0,y_0,y)}, \quad p_0>0, \quad (D1)$$

where

$$h(p_0,y_0,y)=\int_{y_0}^y\frac{dy'}{\tau_{es}(y')\mathcal{P}(p_0,y_0,y')}.$$

If $p_0<0$, one must replace $y\rightleftharpoons y_0$ on the right-hand side of Eq. (D1). If there is a single turning point $y_2^*<y_0$, one can obtain, for $p_0<0$,

$$M(p_0,y_0,y)=\Theta(y-y_2^*)\begin{cases} e^{-h(p_0,y,y_0)}+e^{-h(p_0,y_2^*,y_0)-h(p_0,y_2^*,y)}, & y_2^*<y<y_0 \\ e^{-h(p_0,y_2^*,y_0)-h(p_0,y_2^*,y)}, & y_0<y. \end{cases} \tag{D2}$$

If $y_2^*>y_0$, then, for $p_0>0$,

$$M(p_0,y_0,y)=\Theta(y_2^*-y)\begin{cases} e^{-h(p_0,y_0,y)}+e^{-h(p_0,y_0,y_2^*)-h(p_0,y,y_2^*)}, & y_0<y<y_2^* \\ e^{-h(p_0,y_0,y_2^*)-h(p_0,y,y_2^*)}, & y<y_0. \end{cases} \tag{D3}$$

For the cases $y_2^*<y_0, p_0>0$ and $y_2^*>y_0$, $p_0<0$, one should use formulas for the case without turning points, because under these conditions an electron actually never comes to the turning point. For the case with two turning points (electrons are captured in the potential well) one can find

$$M(p_0,y_0,y)=\frac{\Theta(y-y_{3l}^*)\Theta(y_{3r}^*-y)}{1-e^{-2h(p_0,y_{3l}^*,y_{3r}^*)}}\begin{cases} e^{-h(p_0,y_0,y)}+e^{-h(p_0,y_0,y_{3r}^*)-h(p_0,y,y_{3r}^*)}, & y_0<y<y_{3r}^* \\ e^{-h(p_0,y_0,y_{3r}^*)-h(p_0,y,y_{3r}^*)}+e^{-h(p_0,y_0,y_{3r}^*)-h(p_0,y_{3l}^*,y_{3r}^*)-h(p_0,y_{3l}^*,y)}, & y_{3l}^*<y<y_0 \end{cases} \tag{D4}$$

for $p_0>0$. If $p_0<0$, then

$$M(p_0,y_0,y)=\frac{\Theta(y-y_{3l}^*)\Theta(y_{3r}^*-y)}{1-e^{-2h(p_0,y_{3l}^*,y_{3r}^*)}}\begin{cases} e^{-h(p_0,y,y_0)}+e^{-h(p_0,y_{3l}^*,y_0)-h(p_0,y_{3l}^*,y)}, & y<y_0<y_{3r}^* \\ e^{-h(p_0,y_{3l}^*,y_0)-h(p_0,y_{3l}^*,y)}+e^{-h(p_0,y_{3l}^*,y_0)-h(p_0,y_{3l}^*,y_{3r}^*)-h(p_0,y,y_{3r}^*)}, & y_{3l}^*<y_0<y. \end{cases} \tag{D5}$$

[1] L. L. Chang, L. Esaki, and R. Tsu, Appl. Phys. Lett. **24**, 593 (1974).

[2] T. C. L. G. Solner, E. R. Brown, C. D. Parker, and W. D. Goodhue, in *Electronic Properties of Multilayers and Low-Dimensional Semiconductor Structures*, edited by J. M. Chamberlain *et al.* (Plenum, New York, 1990), p. 283.

[3] F. Capasso, S. Sen, F. Beltram, in *High Speed Semiconductor Devices*, edited by S. M. Sze (Wiley, New York, 1990), p. 465.

[4] A. S. Seabaugh and M. A. Reed, in *VLSI Electronics, Microstructure Science, Vol. 24, Heterostructures and Quantum Devices*, edited by N. G. Einspruch and W. R. Frensley (Academic, New York, 1994), p. 351.

[5] J. Faist *et al.*, Science **264**, 553 (1994).

[6] J. Faist *et al.*, Electron. Lett. **30**, 865 (1994).

[7] R. Tsu and L. Esaki, Appl. Phys. Lett. **22**, 562 (1973).

[8] S. Luryi, Appl. Phys. Lett. **47**, 490 (1985).

[9] L. I. Glazman and R. I. Shekhter, Solid State Commun. **66**, 65 (1988).

[10] N. S. Wingreen, K. W. Jakobsen, and J. W. Wilkins, Phys. Rev. Lett. **61**, 1396 (1988).

[11] B. Ricco and M. Ya. Azbel, Phys. Rev. B **29**, 1970 (1984).

[12] V. J. Goldman, D. C. Tsui, and J. E. Cunningham, Phys. Rev. Lett. **58**, 1256 (1987).

[13] E. S. Alves *et al.*, Electron. Lett. **24**, 1190 (1988).

[14] A. Zaslavski, V. J. Goldman, D. C. Tsui, and J. E. Cunningham, Appl. Phys. Lett. **53**, 1408 (1988).

[15] F. W. Sheard and G. A. Toombs, Appl. Phys. Lett. **22**, 114 (1988).

[16] N. C. Kluksdhal, A. M. Kriman, D. K. Ferri, and C. Righofer, Phys. Rev. B **39**, 7720 (1989).

[17] K. Jensen and F. Buot, Phys. Rev. Lett. **66**, 1078 (1991).

[18] V. I. Ryzhii, V. I. Tolstikhin, I. I. Khmyrova, and O. V. Kosatykh, Mikroelektronika **18**, 147 (1989); V. I. Ryzhii and I. I. Khmyrova, Fiz. Tekh. Poloprovodn, **25**, 637 (1991) [Sov. Phys. Semicond. **25**, 387 (1991)].

[19] H. P. Gibbs, *Optical Bistability: Controlling Light by Light* (Academic, New York, 1985).

[20] C. M. Bowden, H. M. Gibbs, and S. L. McCall, *Optical Bistability 2* (Plenum, New York, 1984).

[21] E. Schöll, *Nonequilibrium Phase Transitions in Semiconductors* (Springer-Verlag, Berlin, 1987).

[22] Z. S. Gribnikov, V. A. Kochelap, and V. V. Mitin, Zh. Eksp. Teor. Fiz. **59**, 1828 (1970) [Sov. Phys. JETP **32**, 991 (1971)].

[23] M. Asche, Solid-State Electron. **32**, 1633 (1989).

[24] H. M. Gibbs *et al.*, Phys. Rev. A **32**, 692 (1985); M. Lindberg, S. W. Koch, and H. Haug, *ibid.* **33**, 407 (1986).

[25] V. A. Kochelap, L. Yu. Melnikov, and V. N. Sokolov, Fiz. Tekh. Poloprovodn. **16**, 1167 (1982) [Sov. Phys. Semicond. **16**, 746 (1982)]; V. A. Kochelap and V. N. Sokolov, *ibid.* **21**, 1324 (1987) [*ibid.* **21**, 805 (1987)]; Phys. Status Solidi B **142**, 311 (1988); **159**, 190 (1990).

[26] V. I. Okulov and V. V. Ustinov, Fiz. Nizk. Temp. **5**, 213 (1979) [Sov. J. Low Temp. Phys. **5**, 101 (1979)].

[27] V. A. Gasparov and R. Huguenin, Adv. Phys. **42**, 393 (1993).

[28] D. H. Chow and J. N. Schulman, Appl. Phys. Lett. **64**, 76 (1994).

[29] M. L. Leadbeater, L. Eaves, M. Henini, O. H. Hughes, G. Hill, and M. A. Pate, Solid-State Electron. **32**, 1467 (1989).

[30] T. Schmidt, M. Teword, R. J. Haug, K. v. Klitzing, B. Schönherr, P. Grambow, A. Föster, and H. Lüt, Appl. Phys. Lett. **68**, 838 (1996).

[31] G. Iannaccone and B. Pellegrini, Phys. Rev. B **52**, 17 406 (1995).

[32] G. Iannaccone and B. Pellegrini, Phys. Rev. B **53**, 2020 (1995).

[33] D. K. Ferry, *Semiconductors* (Macmillan, New York, 1991).